UDK 669.01:62-971
Original scientific article/Izvirni znanstveni članek

ISSN 1580-2949
MTAEC9, 57(6)617(2023)

EFFECT OF STEEL'S THERMAL CONDITION ON THE TRANSFORMATION TEMPERATURES OF TWO HOT-WORK TOOL STEELS WITH INCREASED THERMAL CONDUCTIVITY

VPLIV TOPLOTNEGA STANJA JEKLA NA PREMENSKE TEMPERATURE DVEH ORODNIH JEKEL ZA DELO V VROČEM S POVIŠANO TOPLOTNO PREVODNOSTJO

Tilen Balaško[1*], Jaka Burja[1,2], Jožef Medved[1]

[1]Faculty of Natural Sciences and Engineering, University of Ljubljana, Aškerčeva cesta 12, 1000 Ljubljana, Slovenia
[2]Institute of Metals and Technology, Lepi pot 11, 1000 Ljubljana, Slovenia

Prejem rokopisa – received: 2023-06-05; sprejem za objavo – accepted for publication: 2023-10-04

doi:10.17222/mit.2023.902

The aim of our study was to investigate how different thermal conditions affect the transformation temperatures of two hot-work steels with high thermal conductivity. We focused on two conditions: soft annealing, and quenching and tempering. Soft annealing results in a ferritic steel matrix with spherical carbides, while quenching and tempering result in a fully hardened and tempered martensitic matrix with secondary and tempering carbides. We analysed samples using a simultaneous thermal analysis (STA) and differential scanning calorimetry (DSC) to determine the transformation temperatures. Controlled heating and cooling allowed us to observe the energy changes associated with the phase transformations. The equilibrium temperatures were calculated using the CALPHAD method. Our study investigated the influence of thermal conditions on different transformation temperatures, including solidus/liquidus temperatures, austenite solid transformation temperatures (A_1 and A_3), austenite solidification temperatures and bainite and/or martensite transformation temperatures. A DSC analysis was used to quantitatively measure the transformation temperatures and energy absorption during the endothermic processes (austenite solid transformation and melting) and to study the energy release during the exothermic processes (solidification and transformation). The results showed that soft annealing reduced the solidification interval and the solidus temperature, while energy absorption increased during melting. Conversely, quenching and tempering reduced the austenite solid transformation temperatures and energy release during solidification, including δ-ferrite solidification.

Keywords: thermal analysis, hot-work tool steels, differential scanning calorimetry, heat treatment

Namen naše raziskave je bil raziskati, kako različne toplotne obdelave vplivajo na transformacijske temperature dveh jekel za vroče delo s povišano toplotno prevodnostjo. Osredotočili smo se na dve toplotni obdelavi: mehko žarjene ter kaljene in popuščanje (poboljšanje). Posledica mehkega žarjenja je feritna jeklena matrica s sferičnimi karbidi, medtem ko kaljenje in popuščanje povzroči popolnoma utrjeno in popuščeno martenzitno matrico z enakomerno porazdeljenimi sekundarnimi in popuščnimi karbidi. Vzorce smo analizirali s simultano termično analizo (STA) in diferenčno vrstično kalorimetrijo (DSC), da smo določili transformacijske temperature. Nadzorovano segrevanje in ohlajanje nam je omogočilo opazovanje energijskih sprememb, povezanih s faznimi transformacijami. Ravnotežne temperature smo izračunali z metodo CALPHAD. Naša študija je preučevala vpliv toplotnih obdelav na različne temperature transformacije, vključno s temperaturami solidus/likvidus, temperaturami transformacije avstenita (A_1 in A_3), začetnimi temperaturami strjevanja avstenita in temperaturami transformacije bainita in/ali martenzita. Analiza DSC je bila uporabljena za merjenje transformacijskih temperatur in absorpcije energije med endotermnimi procesi (transformacija avstenita v trdnem in taljenje) ter za študij sproščanja energije med eksotermnimi procesi (strjevanje in transformacija). Rezultati so pokazali, da mehko žarjeno stanje zmanjša interval strjevanja in solidus temperaturo, medtem ko se je med taljenjem povečala absorpcija energije. Nasprotno pa je poboljšano stanje znižalo temperature transformacije avstenita v trdnem in sproščanje energije med strjevanjem, vključno s strjevanjem δ-ferita.

Ključne besede: termična analiza, orodna jekla za delo v vročem, diferenčna vrstična kalorimetrija, toplotna obdelava

1 INTRODUCTION

Tool steels are known for their hardness, wear resistance, resistance to deformation and fracture, and endurance at high temperatures.[1–9] As per the AISI classification system, these steels can be categorized into nine distinct groups, each bearing its own unique designation.[2,7,9] Hot-work tool steels, which bear designation H, find their use in the area of elevated temperatures and are strategically divided into three different groups: chromium, tungsten and molybdenum steels.[1,2,6,7,9] These steels exhibit remarkable resistance to thermal softening at high temperatures and retain their structural integrity during prolonged exposure and/or cyclic temperature changes.[1–9] Group H steels are mainly used for making tools that are used in various processes such as die-casting of light metals, polymer extrusion, forging operations and more.[1–5,9,10] In addition, the new generation of hot-work tool steels exhibits even higher thermal conductivity. Studies have shown that steels with increased thermal conductivity have better mechanical properties at higher temperatures, a longer tool life, better casting quality, higher resistance to thermal fatigue and better cooling performance compared to conventional tool

*Corresponding author's e-mail:
tilen.balasko@ntf.uni-lj.si (Tilen Balaško)

steels.[11–14] Extensive research has highlighted the pronounced influence of Mn, Ni, Mo and Cr on the thermal conductivity of steels.[15,16] For this reason, the steels examined have an increased Mo content.

It is generally accepted that heat treatment processes are essential in the field of hot-work tool steels. As a rule, heat treatment of hot-work tool steels involves two distinct stages: (1) heat treatment during the manufacturing process and (2) final heat treatment, which is usually carried out after machining.[5] From the perspective of end-users, the final heat treatment (2) is of utmost importance, as careful control of this phase ensures the achievement of the desired microstructural components and thus the desired mechanical properties. There are three crucial steps in the final heat treatment: austenitising, quenching and tempering. To achieve the desired mechanical properties, the temperatures, duration of immersion/tempering and cooling rates must be carefully considered. They are the most important parameters to consider.[2,4,5,7,17–19] The fundamental property of steel, together with the complicated interplay of chemical composition, forms the main basis for the remarkable resistance of hot-work tool steels to thermal softening at elevated temperatures.[2,4–6,17] High thermal conductivity hot-work tool steels require a three-step tempering process. A number of studies were carried out to investigate the effects of elevated temperatures on the properties of hot-work tool steels[20–26] and to explore the influence of heat treatment on the microstructure and mechanical properties.[27–33] However, to the best of our knowledge, there is a notable absence of studies exploring the effects of heat treatment on transformation temperatures, including A_1, A_3, M_S, B_S, T_L, T_S, as well as on the austenite solidification temperature, solidification interval and energies absorbed or released during a heating and cooling process of hot-work tool steels. These temperatures are of immense importance, especially in the field of hot-work tool steel use. This is because the proximity of the operating temperature to the start of the transformation to austenite (A_1) has a direct influence on the softening rate when the steel is exposed to elevated temperatures. Typically, these temperatures are determined by quenching the steel at austenitisation temperatures when the microstructure is predominantly austenitic.

Our primary investigation therefore relates to the changes that can be observed at these temperatures when we compare steel in the quenched and tempered condition with steel in the soft annealed condition. In theory these changes should influence the heating/melting stage but not the cooling/solidification stage. This is of particular importance since steels are usually used in the quenched and tempered condition. We are also interested in how these changes affect the energies absorbed and released during a heating and cooling process. Furthermore, this topic is of great importance in the field of 3D printing or additive manufacturing of tool steels as it includes both the energies involved and the transformation temperatures. To investigate these aspects, we performed differential scanning calorimetry (DSC) experiments to explore the influence of heat treatment on the transformation temperatures and energies absorbed or released during heating and cooling cycles. We studied two different hot-work tool steels in two different thermal states. The first condition corresponded to the soft annealed condition, which served as our reference point since tool steels are usually supplied in the "as-delivered" condition, in which the matrix has a ferritic structure and spherical carbides.[7] The second thermal state corresponded to the quenched and tempered (QT) condition, which was characterised by a completely hardened and tempered martensitic matrix, in which secondary and tempering carbides were evenly distributed.[7]

2 EXPERIMENTAL PART

Two high thermal conductivity hot-work tool steels, namely HTCS-130 and W600, were investigated and their chemical compositions are given in **Table 1**. The compositions were determined with a wet chemical analysis and infrared absorption after combustion with ELTRA CS-800.

The heat treatment of the steels studied began with the implementation of the prescribed heat treatment procedures listed in **Table 2**. In all cases, a uniform soaking time of 30 min was used. After quenching in oil, tempering was performed using a Bosio EUP-K 6/1200 chamber furnace. The duration of each tempering stage, for both steels investigated, was 2 h. Due to the air atmo-

Table 1: Chemical compositions of the investigated hot-work tool steels in weight percent

Sample	C	Si	Mn	P	S	Cr	Ni	Mo	V	W	Fe
W600	0.32	0.12	0.23	0.005	0.001	0.11	2.10	3.20	/	1.90	Bal.
HTCS-130	0.31	0.07	0.08	0.007	0.001	0.10	0.04	3.20	0.01	1.90	Bal.

Table 2: Heat treatment processes employed for the steels investigated

Sample	Hardness (HRC)	Austenitization temperature (°C)	First tempering (°C)	Second tempering (°C)	Third tempering (°C)
W600	42–44	1090	540	590	640
HTCS-130	42–44	1080	540	590	640

sphere during heat treatment, the steel surface was milled 2 mm deep to mitigate the effects of decarburisation and oxidation.

To verify the effectiveness of the heat treatment process, Vickers hardness measurements were carried out using an Instron Tukon 2100B instrument. The average values obtained with these measurements are shown in **Table 3**. It is important to note that these values were not included in the analysis of the results as they were only used to confirm the successful completion of the heat treatment and determine different thermal conditions of the steels tested.

Table 3: Measured hardness of the samples

Sample	Hardness (HV 10)
W600	197
W600QT	422
HTCS-130	179
HTCS-130QT	438

The microstructural properties of hot-work tool steels in different thermal states have been well documented. In the soft annealed condition, these steels exhibit a microstructure consisting of a ferritic matrix with carbon chemically bonded in globular carbides.[7] In contrast, the quenched and tempered microstructure exhibits a martensitic matrix with evenly dispersed primary and secondary carbides.[7] In particular, the W600 steel exhibits a microstructure comprising a martensitic matrix together with M_6C ($(Mo,Fe,V)_6C$) and MC ((W,Mo)C) carbides. In addition, traces of (Nb,Cr)CN, (V,Nb)N and TiN (less than 0.1 mass percent) are present in this steel.[34,35] On the other hand, the HTCS-130 steel has a microstructure characterised by a martensitic matrix with small amounts of bainite, accompanied by M_6C ($(Mo,Fe,V)_6C$) and MC ((W,Mo)C) carbides.[36]

After the heat treatment, samples with dimensions of h = 4 mm and Φ = 4 mm were prepared for the subsequent DSC analysis. The DSC analysis was conducted using a NETZSCH STA (simultaneous thermal analyser) Jupiter 449C instrument.

To further improve our understanding, CALPHAD (CALculation of PHAse Diagrams) simulations were carried out with the Thermo-Calc 2023a software, using the TCFE10 (TCS steel and Fe-alloys database) thermodynamic database. The aim of these simulations was to calculate the equilibrium transformation temperatures for the steels studied, thus gaining valuable insights into their thermal behaviour.

The DSC analysis was carried out with the NETZSCH STA Jupiter 449C device under a protective Ar5.0 atmosphere with a constant flow rate of 30 mL·min^{-1}. A standardised temperature programme was used for the steels investigated, with heating and cooling rates set at 10 °C min^{-1}. The samples were heated from room temperature to 1550 °C and then cooled back to room temperature. To ensure accurate measurements, empty Al_2O_3 crucibles were used as the reference material. The masses of the samples were between 390 and 410 mg. By analysing the DSC heating and cooling curves, the experimental transformation temperatures of the steels studied were determined. This method of analysis is widely accepted and is often used to determine the transformation temperatures of various metal alloys.[37–41]

Following the DSC analysis, the samples were prepared for a microstructural analysis by grinding, polishing and etching with Nital. This preparation technique allowed better visibility of the microstructure under a light microscope. The microstructural analysis was performed using a Nikon Microphot FXA microscope equipped with a 3CCD video camera, model Hitachi HV-C20A. Light microscopy served as the primary method for evaluating and examining the resulting microstructure after the DSC analysis.

3 RESULTS AND DISCUSSION

In order to clearly distinguish between the two thermal states of the steels examined, specific names were assigned to them. The steels in the soft annealed condition were named W600 and HTCS-130 (soft annealed), while the steels in the quenched and tempered condition were named W600QT and HTCS-130QT (quenched and tempered). This naming was chosen to avoid confusion or possible errors in the analysis and interpretation of the results. It is important to note that the soft annealed condition reflects the typical condition in which hot-work tool steels are supplied by manufacturers. On the other hand, the term "heat treatment" refers specifically to the quenched and tempered condition, as the soft annealed steels are usually quenched and tempered prior to use to achieve the desired mechanical and other properties.

3.1 CALPHAD calculations

In order to determine the equilibrium transformation temperatures for the steels studied, thorough calculations were carried out. The main focus was on determining the austenite solid transformation temperatures as well as the liquidus, solidus and austenite solidification temperatures.

Two main equilibrium diagrams, known as "property diagrams", were constructed to show the thermodynamically stable equilibrium phases as a function of temperature. These diagrams, shown in **Figure 1**, were calculated based on the specific chemical compositions of the W600 and HTCS-130 steels. Using the data derived from these diagrams, the transformation temperatures were determined for the steels studied. These temperature values were summarised and organised in tables (**Tables 4** and **5**) for an easy reference and analysis.

Upon examining the solidification interval presented in **Table 4**, it can be observed that there are no signifi-

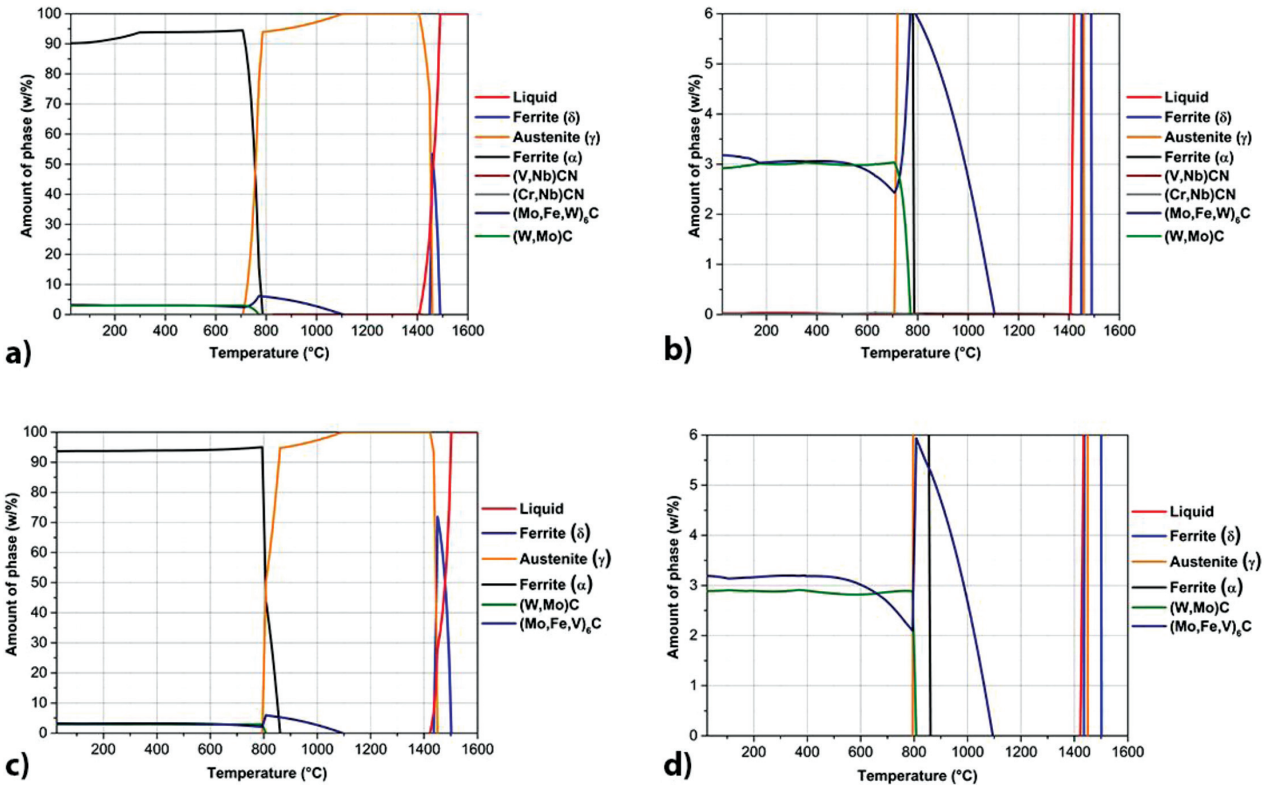

Figure 1: Amounts of all thermodynamically stable equilibrium phases as a function of temperature: a) and b) for W600 steel; c) and d) for HTCS-130 steel

cant differences between the steels studied. This finding is attributed to the fact that the main difference in their chemical composition lies mainly in the Ni content and slightly in the Mn content.

Table 4: Transformation temperatures of the investigated steels, calculated using the CALPHAD method

Sample	Liquidus (°C)	Austenite (°C)	Solidus (°C)	Solidification interval (°C)
W600	1491	1460	1408	83
HTCS-130	1502	1451	1423	79

When examining the austenite solid transformation temperatures, shown in **Table 5**, a remarkable difference is noted. This difference can be attributed to the influence of the chemical composition, in particular the increased Ni content and the slightly increased Mn content in the W600 steel. It appears that the addition of Ni and Mn causes the Ae_1 and Ae_3 temperatures to be lowered while, at the same time, the interval of the two-phase field to be lengthened. The reason for this is that both Ni and Mn are austenite stabilizing elements.

Table 5: Equilibrium temperatures of the austenite solid transformation of the steels examined, calculated using the CALPHAD method

Sample	Ae_1 (°C)	Ae_3 (°C)	Two-phase field interval (°C)
W600	708	785	77
HTCS-130	804	861	57

3.2 DSC analysis

We summarised the results of the differential scanning calorimetry (DSC) analysis in tables and produced diagrams illustrating the heating and cooling curves of all the samples studied. **Figure 2** shows the DSC heating curves, which allow us to determine important temperatures such as the solidus temperature, the austenite solid transformation temperatures (Ac_1 and Ac_3) and the energies absorbed during austenite solid transformation and melting (endothermic processes). Similarly, **Figure 3** shows the DSC curves during cooling, which provide information on the liquidus temperature, the initial temperature of austenite solidification and the initial temperature of bainite transformation. As part of the energy analysis, we can also determine the energies released (exothermic processes) during the solidification of δ-ferrite, austenite and the subsequent bainite transformation.

Let us first examine the effects of heat treatment on the DSC heating curves shown in **Figure 2**. These curves provide valuable information on the solidus temperature, the austenite solid transformation temperatures (Ac_1 and Ac_1) and the energy absorbed during austenite solid transformation and melting, which are representative of endothermic processes. The results obtained from the DSC heating curves are summarised and clearly presented in **Tables 6** and **7**. These tables summarise the measured temperatures and the corresponding energy

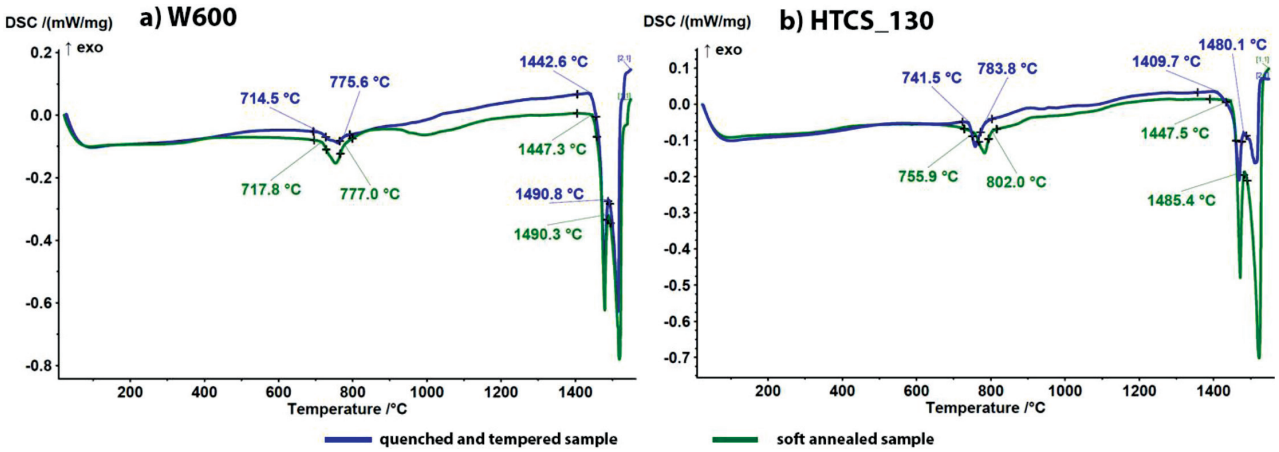

Figure 2: Heating DSC curves of the investigated samples: a) W600 and b) HTCS-130 steels

values associated with the observed thermal transformations.

The results compiled in Table 6 refer to the austenite solid transformation temperatures although in the cases of the W600 and HTCS-130 steels, both temperatures (Ac_1 and Ac_3) are lower for the quenched and tempered sample. The interval of the two-phase field remains almost the same, in the case of the W600 steel, the difference is only 1.9 °C. In the case of HTCS-130, however, the interval of the two-phase field is 3.8 °C smaller for the quenched and tempered sample. The main reason for the differences between the Ac_1 and Ac_3 temperatures of the W600 and HTCS-130 steels is the Ni content, as it stabilizes the γ-region in the phase diagram. The difference in the Mn content also contributes a little, as it is also an austenite stabilizing element.

Table 6: Austenite solid transformation temperatures of the investigated samples, with the corresponding two-phase field interval

Sample	Ac_1 (°C)	Ac_3 (°C)	Two-phase field interval (°C)
W600	717.8	777.0	59.2
W600QT	714.5	775.6	61.1
HTCS-130	755.9	802.0	46.1
HTCS-130QT	741.5	783.8	42.3

The following table (**Table 7**) compiles the energies absorbed during austenite solid transformation and melting. For both steels studied, the energy absorbed during austenite solid transformation is lower for the quenched and tempered samples. However, the difference is the largest for the W600 steel, being –10.216 J·g^{-1}, while the difference for HTCS-130 is minimal. On the other hand, the energies absorbed during melting are also lower for the quenched and tempered samples of both steels. However, the largest difference is found for HTCS-130 where the quenched and tempered sample absorbs –75.53 J·g^{-1} less energy to melt compared to the soft annealed sample.

From the results obtained, it appears that the quenched and tempered samples absorb less energy to melt than the samples in the soft annealed condition. This is to be expected as, from a thermodynamic point of view, the martensitic matrix is less stable during heating than the ferritic matrix; more alloying elements are dissolved in the matrix and the carbides are small and homogeneously distributed in the samples. In contrast, the samples in the soft annealed condition have a thermodynamically stable ferritic matrix with large spherical carbides that are inhomogeneously distributed. It seems that especially an increased Ni content and a slightly increased Mn content influence the austenite solid transformation energies because for the W600 steels the difference between the soft annealed and the quenched and tempered sample was larger compared to HTCS-130. On the other hand, these two elements also influence the melting energy, as the distance between the soft annealed and the quenched and tempered sample was smaller for the W600 steel than for HTCS-130.

Table 7: Absorbed energies during austenite solid transformation and melting (endothermic processes) of the investigated samples

Sample	Energies (J·g^{-1})	
	Austenite solid transformation	Melting
W600	–18.350	–170.4
W600QT	–8.134	–152.3
HTCS-130	–10.210	–158.7
HTCS-130QT	–9.991	–83.17

With the following analysis, we examine the effects of heat treatment on the DSC curves associated with solidification (**Figure 3**). These curves provide a valuable insight into the liquidus temperature, the initial temperature of austenite solidification and the initial temperature at which bainite transformation occurs. By examining the energetic aspects, we can determine the energies released (exothermic processes) during the solidification phases of δ-ferrite and austenite, as well as the energies released during bainite transformation. **Tables 8** to **10** provide a comprehensive summary of the DSC curves obtained during the cooling process.

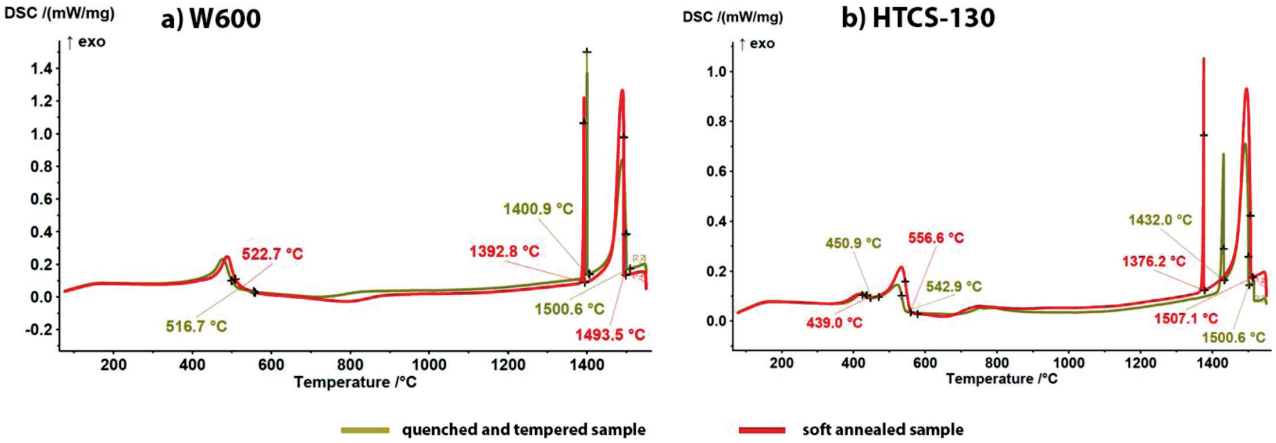

Figure 3: Cooling DSC curves of the investigated samples: a) W600 and b) HTCS-130 steels

First, we investigate the influence of heat treatment on solidification (**Table 8**). The results for the W600 steel show that the quenched and tempered samples have higher liquidus and austenite solidification temperatures compared to the other condition. Conversely, the solidus temperature is slightly lower for the quenched and tempered samples compared to the soft annealed samples. In addition, the solidification interval is larger for the quenched and tempered samples, with a difference of 11.8 °C. Similar trends can be observed for the HTCS-130 steel where the solidification interval is even larger than for the W600 steel, 31.3 °C. This also shows that the quenched and tempered samples have higher austenite solidification temperatures but lower solidus temperatures.

In both cases, however, the solidification interval is wider in the samples subjected to quenching and tempering. The main difference lies in the austenite solidification temperature, which is particularly pronounced in the HTCS-130 steel. From the results, it appears that both alloying elements (Ni and Mn) influence the solidification interval, which is narrower for W600 than for HTCS-130 in both thermal conditions. The difference becomes even more evident when comparing the solidification intervals of both steels under both thermal conditions, where W600 has an interval of 11.8 °C and HTCS-130 has an interval of 31.3 °C.

Table 8: Liquidus, solidus and austenite solidification temperatures, with the corresponding solidification interval of the investigated samples

Sample	Liquidus (°C)	Austenite (°C)	Solidus (°C)	Solidification interval (°C)
W600	1493.5	1392.8	1447.3	46.2
W600QT	1500.6	1400.9	1442.6	58.0
HTCS-130	1507.1	1376.2	1447.5	59.6
HTCS-130QT	1500.6	1432.0	1409.7	90.9

We continue with the results concerning the energies released (exothermic processes) obtained when cooling the samples (**Table 9**). For both steels studied, less energy is released during δ-ferrite formation and complete solidification for the samples in the quenched and tempered condition. Furthermore, the energy released during bainite transformation is almost the same for the W600 steel in both thermal states. However, for the HTCS-130 steel, ferrite precipitation occurs before bainite transformation. The energy released during ferrite and bainite transformation is lower for the quenched and tempered sample. There is no ferrite precipitation in W600, which is due to the high Ni content. The energy during austenite solidification is almost the same in both thermal states of the W600 steel. Minor differences occur in the HTCS-130 steel where more energy is released for the quenched and tempered sample (4.84 $J \cdot g^{-1}$).

If we look only at the total solidification and compare the results for both steels, it is obvious that in the case of the W600 steel there is little change between the two thermal states compared to the results for HTCS-130.

Table 9: Released energies during solidification and bainite transformation (exothermic processes) of the investigated samples

Sample	Energies ($J \cdot g^{-1}$)			
	δ-ferrite solidification	γ-austenite solidification	Entire solidification (δ-ferrite and γ-austenite)	Bainite transformation
W600	141.00	13.05	154.05	65.39
W600QT	109.20	13.41	122.61	66.29
HTCS-130	135.10	11.28	146.38	78.84
HTCS-130QT	87.11	16.12	103.23	51.64

At the end of cooling, another peak can be analysed on the DSC curves of cooling, which belongs to the bainite transformation (**Table 10**). For the W600 steel, we are able to determine the initial bainite transformation temperature, which is slightly higher for the soft annealed sample with only a 6 °C difference. The results for the HTCS-130 steel are different as there are two peaks on the DSC cooling curve. The first belongs to the temperature of ferrite precipitation. The initial ferrite precipitation temperature is 13.5 °C higher for the soft annealed sample. The second peak, which is just below

the ferrite precipitation temperature, belongs to bainite transformation. This is also confirmed by light microscopy (**Figure 5**) where ferrite can be found along the grain boundaries.

For the HTCS-130 steel, the ferrite precipitation temperature is higher for the quenched and tempered sample, and the metallographic analysis also showed more ferrite than for the soft annealed sample. For the W600 steel, the initial bainite transformation temperatures are almost the same for the samples in the two thermal states and the interval for the two-phase field is also almost the same in both cases (**Table 7**). It seems that the addition of Ni and Mn suppresses the ferrite precipitation when we compare the results for the W600 and HTCS-130 steels.

Table 10: Starting temperatures of bainite transformation of the investigated samples and ferrite precipitation along the austenite grain boundaries for the HTCS-130 steel

Sample	Ferrite precipitation (°C)	B_S (°C)
W600	/	522.7
W600QT	/	516.7
HTCS-130	556.6	439.0
HTCS-130QT	543.1	450.9

3.3 Light microscopy

Due to the peaks on the DSC cooling curve below 550 °C (**Figure 3** and **Table 10**), we also performed light microscopy to clarify, which transformation these peaks belong to. As with the microstructures obtained with the light microscope (**Figures 4** and **5**), an additional explanation is first required to clarify why both dark and light areas are labelled as bainite. The reason is the etching effect, which varies due to the orientation of bainite nee-

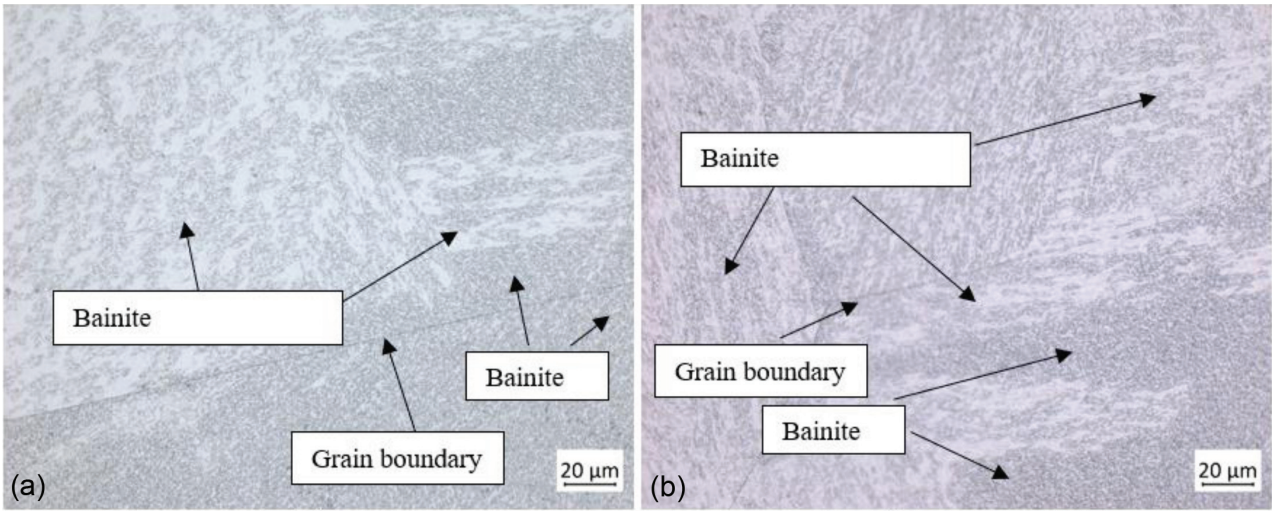

Figure 4: Microstructure of the W600 steel: a) soft annealed sample and b) quenched and tempered sample

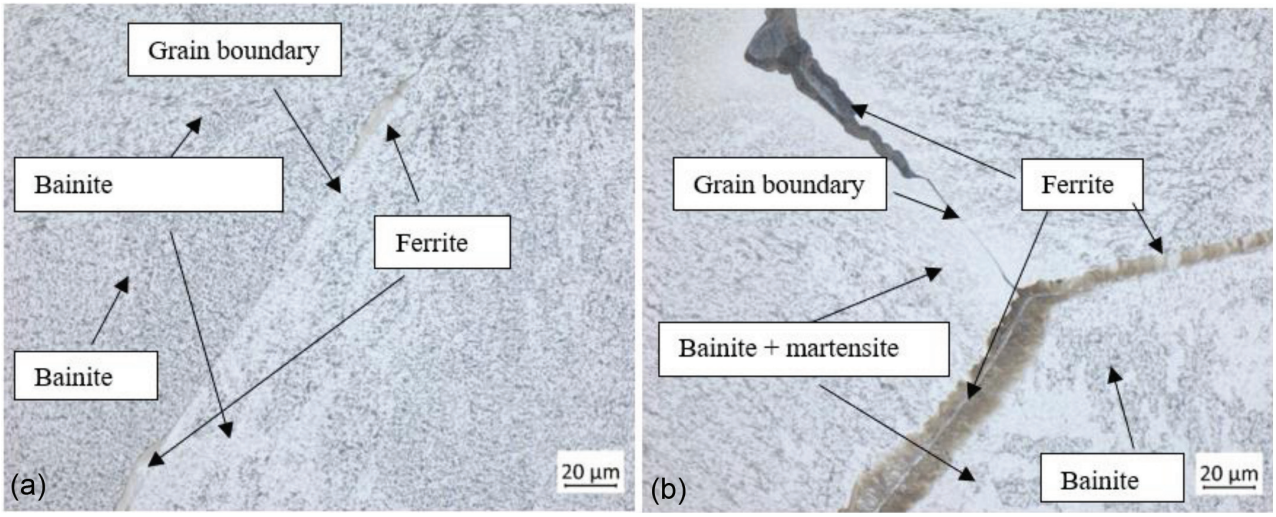

Figure 5: Microstructure of the HTCS-130 steel: a) soft annealed sample and b) quenched and tempered sample

dles and makes some areas appear lighter and others darker. The following figure (**Figure 4**) shows the microstructure of the samples after the DSC analysis for the W600 steel in the soft annealed condition (**Figure 4a**) and quenched and tempered condition (**Figure 4b**). Based on the evaluation of the microstructure in both states, the peaks (**Table 10**) belong to the bainite transformation temperatures.

The next figure (**Figure 5**) shows the microstructure of the HTCS-130 steel after the DSC analysis in the soft annealed condition (**Figure 5a**) and quenched and tempered condition (**Figure 5b**). Based on the results of the DSC analysis (**Table 10**), two peaks appear in this case. After the microstructural analysis, we found that the first peak belongs to the ferrite precipitation temperature along the austenite grain boundaries in both cases, as shown in **Figure 5**. The second peak, on the other hand, belongs to the bainite transformation temperature, as is the case with the W600 steel.

3.3 Scanning electron microscopy (SEM)

To confirm that ferrite is present along the austenite grain boundaries in the HTCS-130 steel, an additional SEM analysis was carried out. Using EDS (energy-dispersive X-ray spectroscopy) we analysed the areas along the grain boundaries and in the grains, i.e., the matrix. The values of the analysed alloying elements are given in *w*/%. First, we analysed the sample in the soft annealed condition (**Figure 6**) where Area 1 represents the analysed area along a grain boundary while Area 2 represents the area in a grain, i.e., the matrix, which is bainitic, as already confirmed by light microscopy (**Figure 5**). Increased amounts of Mo and W are present along the grain boundary (**Figure 6** – Area 1) when compared with those in the grain (**Figure 6** – Area 2), i.e., the matrix (bainite). Based on these results, we can confirm that ferrite is present along the austenite grain boundaries because it is a known metallurgical fact that both chemical elements (Mo and W) are alphagenic, i.e., they stabilise and support the formation of ferrite.

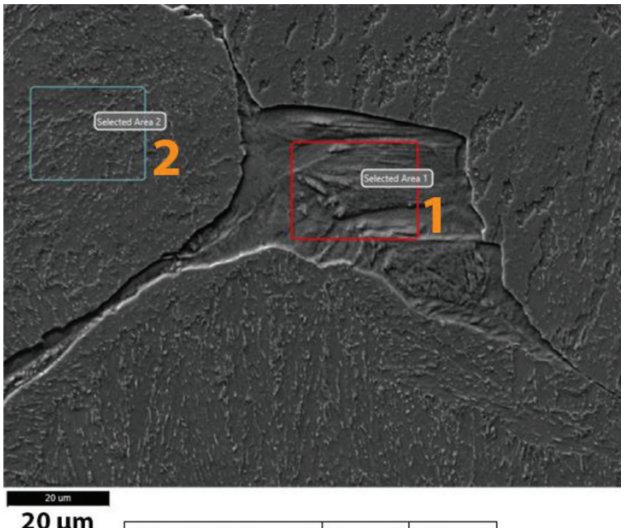

Chemical element	Area 1	Area 2
Fe	92.1	95.4
Mo	5.1	2.9
W	2.8	1.7

Figure 6: EDS-analysed areas with the corresponding chemical compositions in *w*/% for the HTCS-130 steel in the soft annealed condition

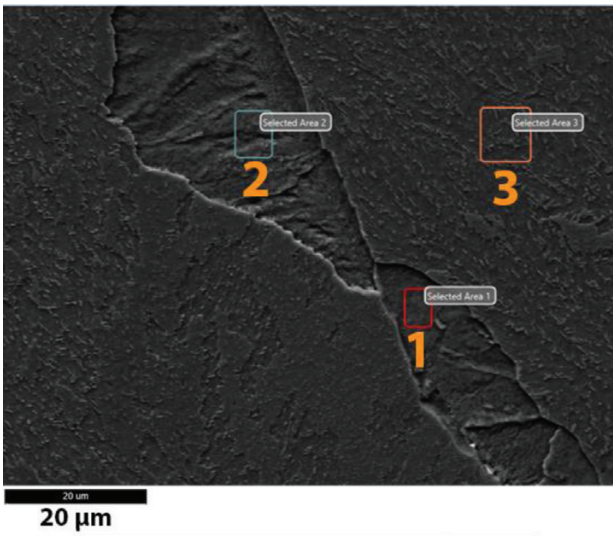

Chemical element	Area 1	Area 2	Area 3
Fe	92.8	93.6	94.9
Mo	4.9	4.4	3.2
W	2.3	2.0	1.9

Figure 7: EDS-analysed areas with the corresponding chemical compositions in *w*/% for the HTCS-130QT steel in the quenched and tempered condition

In the next figure (**Figure 7**), the sample in the quenched and tempered condition is analysed. In this case, Areas 1 and 2 represent the analysed area along a grain boundary and Area 3 represents the area in a grain, i.e., the matrix, which is bainitic, as already confirmed by light microscopy (**Figure 5**). The results are essentially the same as for the sample in the soft annealed condition. There are increased amounts of Mo and W along the grain boundary (**Figure 7** – Areas 1 and 2) when compared with those in the grain (**Figure 7** – Area 3), i.e., the matrix (bainite). Based on these results, we can again confirm that ferrite is present along the austenite grain boundaries. The reasons for this have already been explained in **Figure 6**.

4 CONCLUSIONS

In summary, we can conclude the following:

- Melting is influenced by the initial thermal condition, with the samples in the soft annealed condition con-

suming more energy to melt than the samples in the quenched and tempered condition;
- during melting, increased amounts of Ni and Mn (W600 steel) also increase the energy consumed during melting compared to the energy consumed during the melting of HTCS-130 steel;
- quenching and tempering reduce the austenite solid transformation temperatures in both steels investigated. However, the interval of the two-phase field remains almost unchanged for both steels under both conditions analysed;
- increased amounts of Ni and Mn (W600 steel) also reduce both austenite solid transformation temperatures (Ac_1 and Ac_3), compared to those determined in the case of the HTCS-130 steel;
- the specimens in the soft annealed condition have a lower solidification interval and lower solidus temperatures. At the same time, the austenite solidification temperatures are higher for quenched and tempered samples in both cases. However, there are no major deviations in the liquidus temperatures;
- the energies released during the solidification of the quenched and tempered samples are lower than those required for the soft annealed samples;
- the same tendency is observed during both solidification and melting, i.e., higher amounts of Ni and Mn (W600 steel) also increase the energies released during solidification compared to those released during the solidification of the HTCS-130 steel;
- we were able to determine the initial temperatures of the bainite transformation;
- in the case of the W600 steel, the addition of Ni and Mn suppresses the ferrite precipitation that occurs in the HTCS-130 steel;
- the calculated liquidus temperatures in the case of the HTCS-130 steel are closer to those determined for the quenched and tempered samples, but on the other hand, the calculated liquidus temperatures in the case of the W600 steel are closer to those determined for the soft annealed condition;
- the solidus temperatures of the quenched and tempered samples of both steels investigated are closer to the calculated temperatures;
- meanwhile, the solidification intervals of the quenched and tempered samples are closer to the calculated values for both steels investigated.

5 REFERENCES

[1] C. R. Sohar, Lifetime controlling defects in tool steels, Springer, Berlin 2011, 224

[2] G. Roberts, G. Krauss, R. Kennedy, Tool Steels, 5th ed., ASM International, Materials Park 1998, 364

[3] W. F. Hosford, Iron and Steel, Cambridge University Press, Cambridge 2012, 310

[4] Heat Treater's Guide: Practices and Procedures for Irons and Steels, ASM International, Metals Park 1995, 904

[5] R. A. Mesquita, K. Michael, R. Schneider, Tool steels: properties and performance, CRC Press, Boca Raton 2017, 245

[6] ASM Handbook, Volume 1: Properties and Selection: Irons, Steels, and High-Performance Alloys, ASM International, Materials Park 1990, 1063

[7] C. Højerslev, Tool steels, Risø National Laboratory, Roskilde 2001, 25, http://orbit.dtu.dk/files/7728903/ris_r_1244.pdf, January 2021

[8] H. M. Cobb, Steel products manual: tool steels, Iron and Steel Society, Warrendale 2000, 79

[9] N. Sandberg, On the Machinability of High Performance Tool Steels, Doctoral thesis, Acta Universitatis Upsaliensis, 2012, 58, https://www.diva-portal.org/smash/get/diva2:514634/FULLTEXT01.pdf, 05.08.2012

[10] J. Sjöström, Chromium martensitic hot-work tool steels – damage, performance and microstructure, Doctoral thesis, Karlstad University, 2004, 53, http://www.diva-portal.org/smash/get/diva2:24899/FULLTEXT01.pdf, 21.01.2013

[11] Z. Taha, A. R. Yusoff, M. F. Mohamd Sharif, M. A. H. Saharudin, M. F. Zamri, Comparison of Cooling Performance between High Thermal Conductivity Steel (HTCS 150) and Hot Work Tool Steel (SKD 61) Insert for Experimental Tool Using Finite Element Analysis, Adv. Mater. Res., 903 (**2014**), 163–168, doi:10.4028/www.scientific.net/AMR.903.163

[12] M. Ayabe, T. Nagaoka, K. Shibata, H. Nozute, H. Koyama, K. Ozaki, T. Yanagisawa, Effect of high thermal conductivity die steel in aluminum casting, Int. J. Met., 2 (**2008**), 47–55, doi:10.1007/BF03355427

[13] S. Li, X. Wu, X. Li, X. He, High temperature performance of a Mo-W type hotwork die steel of high thermal conductivity, Chinese J. Mater. Res., 31 (**2017**), 32–40, doi:10.11901/1005.3093.2016.037

[14] I. Valls, A. Hamasaiid, A. Padré, High Thermal Conductivity and High Wear Resistance Tool Steels for Cost-Effective Hot Stamping Tools, J. Phys. Conf. Ser., 896 (**2017**), doi: 10.1088/1742-6596/896/1/012046

[15] M. Peet, H. Hasan, H. Bhadeshia, Prediction of thermal conductivity of steel, Int. J. Heat Mass Transf., 54 (**2011**) 11–12, 2602–2608, doi:10.1016/j.ijheatmasstransfer.2011.01.025

[16] A. R. Zulhishamuddin, S. N. Aqida, An overview of high thermal conductive hot press forming die material development, J. Mech. Eng. Sci., 9 (**2015**), 1686–1694, doi:10.15282/jmes.9.2015.14.0162

[17] G. Krauss, Steels: Processing, Structure, and Performance, ASM International, Materials Park 2015, 682

[18] G. E. Totten, Steel Heat Treatment: Metallurgy and Technologies, CRC Press, Boca Raton 2006, 848

[19] G. N. Haidemenopoulos, Physical Metallurgy: Principles and Design, CRC Press, Boca Raton 2018, 476

[20] Q. Zhou, X. Wu, N. Shi, J. Li, N. Min, Microstructure evolution and kinetic analysis of DM hot-work die steels during tempering, Mater. Sci. Eng. A, 528 (**2011**) 18, 5696–5700, doi:10.1016/j.msea.2011.04.024

[21] A. Medvedeva, J. Bergström, S. Gunnarsson, J. Andersson, High-temperature properties and microstructural stability of hot-work tool steels, Mater. Sci. Eng. A, 523 (**2009**) 1–2, 39–46, doi:10.1016/j.msea.2009.06.010

[22] Z. Zhang, D. Delagnes, G. Bernhart, Microstructure evolution of hot-work tool steels during tempering and definition of a kinetic law based on hardness measurements, Mater. Sci. Eng. A, 380 (**2004**) 1, 222–230, doi:10.1016/j.msea.2004.03.067

[23] N. Mebarki, D. Delagnes, P. Lamesle, F. Delmas, C. Levaillant, Relationship between microstructure and mechanical properties of a 5% Cr tempered martensitic tool steel, Mater. Sci. Eng. A, 387–389 (**2004**) 1–2, 171–175, doi:10.1016/j.msea.2004.02.073

[24] A. Jilg, T. Seifert, Temperature dependent cyclic mechanical properties of a hot work steel after time and temperature dependent softening, Mater. Sci. Eng. A, 721 (**2018**), 96–102, doi:10.1016/j.msea.2018.02.048

[25] D. Caliskanoglu, I. Siller, R. Ebner, H. Leitner, F. Jeglitsch, W. Waldhauser, Thermal Fatigue and Softening Behavior of Hot Work Tool Steels, Proc. 6th Int. Tool. Conf., Karlstad 2002, 707–719

[26] R. Markežič, N. Mole, I. Naglič, R. Šturm, Time and temperature dependent softening of H11 hot-work tool steel and definition of an anisothermal tempering kinetic model, Mater. Today Commun., 22 (**2020**), 1–7, doi:10.1016/j.mtcomm.2019.100744

[27] S. Kheirandish, H. Saghafian, J. Hedjazi, M. Momeni, Effect of heat treatment on microstructure of modified cast AISI D3 cold work tool steel, J. Iron Steel Res. Int., 17 (**2010**), 40–45, doi:10.1016/S1006-706X(10)60140-9

[28] C. J. Chen, K. Yan, L. Qin, M. Zhang, X. Wang, T. Zou, Z. Hu, Effect of Heat Treatment on Microstructure and Mechanical Properties of Laser Additively Manufactured AISI H13 Tool Steel, J. Mater. Eng. Perform., 26 (**2017**) 11, 5577–5589, doi:10.1007/s11665-017-2992-0

[29] M. Priyadarshini, A. Behera, C. K. Biswas, D. K. Rajak, Experimental Analysis and Mechanical Characterization of AISI P20 Tool Steel Through Heat-Treatment Process, J. Bio- Tribo-Corrosion, 8 (2022) 1, 1–10, doi:10.1007/s40735-021-00607-3

[30] F. Huber, C. Bischof, O. Hentschel, J. Heberle, J. Zettl, K. Y. Nagulin, M. Schmidt, Laser beam melting and heat-treatment of 1.2343 (AISI H11) tool steel – microstructure and mechanical properties, Mater. Sci. Eng. A, 742 (**2018**), 109–115, doi:10.1016/j.msea.2018.11.001

[31] I. Souki, D. Delagnes, P. Lours, Influence of heat treatment on the fracture toughness and crack propagation in 5% Cr martensitic steel, Procedia Eng., 10 (**2011**), 631–637, doi:10.1016/j.proeng.2011.04.105

[32] N. B. Dhokey, S. S. Maske, P. Ghosh, Effect of tempering and cryogenic treatment on wear and mechanical properties of hot work tool steel (H13), Mater. Today Proc., 43 (**2021**), 3006–3013, doi:10.1016/j.matpr.2021.01.361

[33] W. R. Prudente, J. F. C. Lins, R. P. Siqueira, P. S. N. Mendes, R. E. Pereira, Microstructural evolution under tempering heat treatment in AISI H13 hot-work tool steel, Int. J. Eng. Res. Appl., 7 (**2017**) 4, 67–71, doi:10.9790/9622-0704046771

[34] T. Balaško, M. Vončina, J. Medved, Simultaneous thermal analysis of the high-temperature oxidation behaviour of three hot-work tool steels, J. Therm. Anal. Calorim., 148 (**2022**), 1251–1264, doi:10.1007/s10973-022-11616-w

[35] T. Balaško, M. Vončina, J. Burja, B. Šetina Batič, High-Temperature Oxidation Behavior of Tool Steel with Increased Thermal Conductivity, Oxid. Met., 98 (**2022**), 135–161, doi:10.1007/s11085-022-10119-1

[36] K. Grabnar, J. Burja, T. Balaško, A. Nagode, J. Medved, The Influence of Nb, Ta and Ti Modification on Hot-work Tool-steel Grain Growth During Austenitization, Mater. Tehnol., 56 (**2022**) 3, 331–338, doi:10.17222/mit.2022.486

[37] E. Kaschnitz, P. Hofer-Hauser, W. Funk, Electrical resistivity measured by millisecond pulse-heating in comparison to thermal conductivity of the hot work tool steel AISI H11 (1.2343) at elevated temperature, High Temp. - High Press., 49 (**2020**) 1–2, 75–87, doi:10.32908/hthp.v49.825

[38] T. Balaško, J. Burja, J. Medved, Effect of Ni on solidification of duplex low-density steels, J. Therm. Anal. Calorim., 142 (**2020**) 5, 1605–1611, doi:10.1007/s10973-020-10254-4

[39] E. Wielgosz, T. Kargul, Differential scanning calorimetry study of peritectic steel grades, J. Therm. Anal. Calorim., 119 (**2015**) 3, 1547–1553, doi:10.1007/s10973-014-4302-5

[40] B. Smetana, M. Žaludová, S. Zlá, J. Dobrovská, M. Cagala, I. Szurman, D. Petlák, Application of high temperature DTA technique to Fe based systems, Proc. of the 19th Int. Metallurgical and Materials Conference, Roznov pod Radhostem 2010, 357–362

[41] B. Smetana, S. Zlá, J. Dobrovská, P. Kozelsky, Phase transformation temperatures of pure iron and low alloyed steels in the low temperature region using DTA, Int. J. Mater. Res., 101 (**2010**) 3, 398–408, doi:10.3139/146.110283